Error assessment and mitigation for hyper-temporal UAV-borne LiDAR surveys of forest inventory.

Luke Wallace[1], Arko Lucieer[1], Darren Turner[1] & Christopher Watson[1]

[1]School of Geography and Environmental Studies, University of Tasmania
Luke.Wallace@utas.edu.au

Abstract

Remotely sensed LiDAR data has become an important tool in the management of modern forest inventories. Monitoring the high frequency changes within forests with this data has been restricted by the cost and intermittent nature of LiDAR surveys. The use of Unmanned Aerial Vehicles (UAVs) as a remote sensing platform is a rapidly developing field and is capable of allowing highly dynamic environmental changes to be monitored. As such recent studies presented in the literature highlight the potential of UAV systems for forest monitoring. This study further investigates the potential of UAVs by examining the achievable accuracy of a newly developed UAV-borne LiDAR system in comparison to a traditional full scale system. The major contributions to the error budget of a UAV-borne LiDAR system are constrained through the use of a novel UAV specific processing workflow. Central to this workflow is the fusion of observations from a low cost Inertial Measurement Unit, a GPS receiver and a high definition video camera with a Sigma-Point Kalman Smoother allowing for highly accurate estimates of orientation. We found that using this workflow and under certain flying conditions accuracies similar to a modern full-scale system are achievable from this low-cost platform.

Key Words: Unmanned Aerial Vehicles, UAV, LiDAR, Accuracy, Error Propagation.

1. Introduction

Airborne LiDAR remote sensing has become an important tool in the management of modern forest inventories (Hyyppä et al. 2008). Ongoing research into the processing and analysis of LiDAR data has allowed for the development of an extensive array of LiDAR derived data products from which a wide range of forest metrics can be derived (Akay et al. 2009). Stand metrics and tree-level statistics derived from LiDAR have provided forest managers with significantly richer information about their forests (Lim et al. 2003; Morsdorf et al. 2009). It is however evident that the full potential of LiDAR technology for forest measurement and management is yet to be reached. Prohibitive factors such as high survey costs and short flying seasons, in many areas, have meant that assessing factors such as forest health, defoliation and rate of canopy closure are not feasible from the current intermittent LiDAR surveys utilised by forest managers.

Recently, improvements in small scale positioning technology have enabled the use of Unmanned Aerial Vehicles (UAVs) as a remote sensing platform offering a distinctive combination of very high resolution data capture at a significantly lower survey cost to traditional platforms. Jaakkola et al. (2010) provided the first example of the potential of this technology for use within the forest industry. By deploying a rotor wing UAV equipped with a number of positioning sensors, in combination with two on-board LiDAR sensors, Jaakola et al. (2010) produced high-resolution data sets capable of individual tree level mapping. Both Jaakkola et al. (2010), and more recently, Lin et al. (2011), have shown that due to the improved density of a UAV captured LiDAR point cloud several metrics (in particularly individual tree

heights) can be measured at a finer scale and with higher precision using already developed processing algorithms when compared to traditional LiDAR platforms. Because of their high spatial and temporal resolution, together with low operation costs, UAVs can provide a more targeted approach to forest monitoring and allow for the use of multi-temporal surveys such as forest health and canopy closure monitoring. Studies such as Jakkola et al. (2010) and Lin et al. (2011) suggest that the combination of low cost, high resolution data capture, UAV platforms are likely to be the next tool of choice for optimising detailed small area surveys within forests.

Current research into the use of UAVs as a 3D data-capture platform includes application specific use in a variety of different fields ranging including for agriculture crop monitoring (Hunt Jr et al. 2010; Berni et al. 2009) to archaeology surveys (Eisenbeiss and Zhang 2006) for example. Despite significant developments into the use of UAVs for 3D mapping, a rigorous analysis of the error structure present within a UAV LiDAR based platform, and how these errors propagate into the final 3D measurements has yet to be undertaken. Such an analysis of error is necessary for use in forestry due to the use of UAV platforms for multi-temporal surveys and the need to distinguish small scale change from error. This paper presents an analysis of the propagation of error based on the stochastic error model of a UAV-borne LiDAR system developed at the University of Tasmania using lightweight, low-cost sensors. In this analysis, we make use of the well-known error propagation techniques used for full-scale traditional LiDAR systems to determine the achievable accuracy under a standard LiDAR processing algorithm and highlight the major sources of error. One of the novel contributions of this paper is in the development of an accurate position and attitude determination framework based on the use of a low cost Inertial Measurement Unit, High Definition video and a Sigma-Point Kalman Smoothing (SPKS).

2. Methods

2.1 Equipment

The low-cost multi-rotor UAV (Droidworx/Mikrokopter AD-8) currently under development by the TerraLuma research group at the University of Tasmania will be used for this study (Figure 1). In comparison to other UAV platforms multi-rotor UAVs offer increased stability and decreased vibration making it the ideal UAV for LiDAR mapping. However, the main drawback of multi-rotor UAVs is their limited payload. In the case of the TerraLuma UAV this is 2.8 kg, which when the primary sensor (Ibeo LUX Automotive Laser Scanner, 1 kg), batteries and logging equipment are taken into account allows for only a minimal payload for position and attitude sensors. Based on these requirements (and a desire to minimise cost) a lightweight sensor suite has been designed consisting of a Microstrain 3DM-GX2 MEMs based Inertial Measurement Unit (IMU) (50 g), a Novatel OEMV-1DF dual-frequency GPS receiver (21.5g + 113 g antenna) and a ContourGPS digital video camera (150 g).

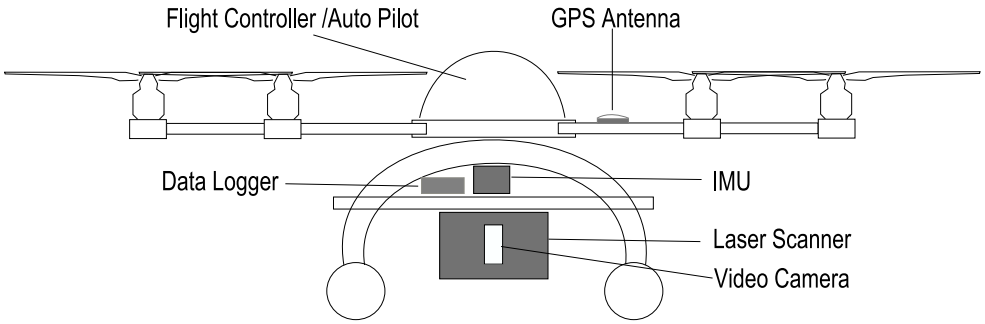

Figure 1. Schematic of the TerraLuma UAV remote sensing platform under development at the University of Tasmania.

The sensor payload is mounted on the UAV through a rigid sensor framework designed such that the lever arm offsets between the LiDAR, IMU, GPS and video camera are minimised and constant. The frame also allows for an adequate sky-view for the accurate operation of both the GPS antenna and GPS enabled video camera. The properties of each sensor have been rigorously tested in order to independently determine their standalone accuracy values under flight conditions. The results from these tests are displayed in Table 1 along with a brief explanation of the methods used to determine the estimates of instantaneous accuracy. Each sensor has been chosen to minimise both cost and weight while providing sufficient resolution and accuracy. All data logging and time synchronisation is performed using an on-board miniaturised computer (Gumstix Verdex pro). All other processing is completed offline.

Table 1: Description of the sensors mounted on-board the TerraLuma UAV and the method used to determine the accuracy of the sensor.

Equipment	Description and Accuracy Determination	Data Rate (Hz)	Standalone Accuracy
Dual-Frequency GPS receiver	Provides 3D positional observation of the helicopter operating under typical short baseline (<3 km) configurations. The GPS receiver has been benched marked against a geodetic grade GPS receiver.	20	**Horizontal** +/- 0.03 m **Vertical** +/- 0.05 m
Microstrain 3DM-GX2 IMU	A light weight - IMU consisting of MEMs based accelerometer, gyroscope and magnetometer triads. An independent calibration procedure following the methods of Zhang et al. (2010) has been performed to verify the calibration and accuracy of the sensor.	100	**Orientation** +/- 2.0 ^{o} (+ bias instabilities and noise)
ContourGPS HD video camera	A high definition video camera equipped with a GPS antenna allowing accurate time synchronisation with the other sensors. The video camera has been calibrated and lens distortions removed using the procedure described by Bouguet (2010). The accuracy of the orientation as determined by video observation has been quantified using dense ground control as reference.	30	**Orientation** +/- 0.2 - 0.5 ^{o}
Ibeo LUX laser Scanner	The Ibeo LUX sensor measures points in four scanning layers and in doing so can record up to 22000 returns/sec. The scanner has a measurement range of up to 200 m. The beam divergence of the Ibeo LUX laser scanner is 0.08^{o} horizontally and 1.6^{o} vertically.	880 (per scan layer)	**Range** +/-0.1 m

2.2 Airborne LiDAR Error Propagation

The calculation of the ground coordinates from the UAV-borne LiDAR system observations follow the same methodology as used for full scale traditional platforms. Coordinates of points that reflect the outbound laser pulse can be calculated directly from the range measurement from the LiDAR sensor, combined with data from the Positioning and Orientation System (POS) on board the UAV using the well known "LiDAR equation" (Eqn 1) (Baltsavias, 1999).

$$\begin{bmatrix} x \\ y \\ z \end{bmatrix} = \begin{bmatrix} X \\ Y \\ Z \end{bmatrix} + R_b^m [R_s^b r^s + a^b] \quad (1)$$

Where:

$[X \quad Y \quad Z]^T$	is the position vector as measured by the POS system expressed in the Earth Centred, Earth Fixed (ECEF) cartesian frame;
R_b^m	is the attitude matrix as measured by the POS and parameterized by the pitch, roll and yaw angles;
R_s^b	is the boresight matrix describing the angular offset between the body frame and the LiDAR frame;
r^s	is the observation vector from the Ibeo LUX system and consists of a range observation as well as an encoder angle; and
a^b	is the lever arm offset between the origin of the POS frame and the LiDAR frame.

There has been significant and ongoing research into the various factors that affect the accuracy of coordinates derived from a LiDAR system (Schaer et al., 2007). Individual LiDAR systems will also contain unique factors that affect the overall error (see May & Toth, 2007 and Morin, 2002 for an overview). However, these errors can be summarised into 17 error components which will occur in every system. These error components and can be described as:

- 3 errors existing in the measurement of the absolute position (σx, σy and σz);
- 3 errors existing in the measurement of aircraft orientation (σω, σφ and σκ);
- 6 errors caused by the inaccurate calibration of the system affecting the boresight angles ($\sigma\omega_b$, $\sigma\varphi_b$ and $\sigma\kappa_b$) and lever arm offset (σx_L, σy_L and σz_L);
- 3 Internal LiDAR System errors occur in measurements of range (σr) and the two encoder angles (σβ and σγ) measured from the UAV; and
- 2 errors due to divergence of the laser beam which propagate in the horizontal direction (σB_h) and elevation angle measurements within the laser scanner reference frame (σB_e). These errors will be modelled as one quarter of the quoted beam divergence of the laser scanner following Lichti and Gordon (2004) and Glennie (2007).

These error components can be propagated through the functional model of the LiDAR system equation enabling the magnitude of the error in the final coordinates of a point to be determined. Propagation for an individual LiDAR strike can be performed by linearising equation 1, through the truncation of the Taylor series expansion after the 1st term and assuming that each of the error sources are uncorrelated (Schaer et al., 2007). This enables the determination of the 3x3 point covariance matrix C_{xyz}, using equation 2 as follows:

$$C_{xyz} = \begin{bmatrix} C_x & C_{xy} & C_{xz} \\ C_{yx} & C_y & C_{yz} \\ C_{zx} & C_{zy} & C_z \end{bmatrix} = F_{ll} C {F_{ll}}^T \quad (2)$$

Where:

F_{ll}	is the Jacobian matrix of the linearised functional model; and
C	is the stochastic model given by a diagonal matrix containing the magnitude of the 17 summarised error sources.

This covariance matrix can be used a-priori to a LiDAR survey in order to determine the best

and worst case point positioning accuracy. The analysis in this report will consider a scenario based on typical UAV flying heights (e.g. 30 – 120 m Above Ground Level), with the aircraft flying a flat northern path (i.e. ω, φ and $\kappa = 0^{o}$). Furthermore, it will be assumed that the observation of a LiDAR measurement has coincided directly with observations of position and orientation from which the expected accuracy of a single LiDAR measurement from this system can be simulated.

2.3 Data Processing and Calibration

The UAV's position and orientation system consists of three sensors (IMU, video, and GPS), providing observations at variable rates up to 200Hz. The rate of the LiDAR sensor, however, is significantly faster, measuring up to 22,000 returns per second. Therefore, the observations from these sensors are required to be interpolated in order to determine the position and orientation of the LiDAR sensor at the instant of each range observation. The most commonly used algorithm for this purpose is the Extended Kalman Filter (EKF), which is limited by its complexity and in its accuracy by the inclusion of a first order linearisation of the functional model (Van Der Merwe & Wan, 2004). To overcome these limitations, the fusion of the positional data for the TerraLuma UAV is completed with the use of a loosely coupled Sigma-Point Kalman smoother (SPKS). It has been shown that variants of SPKS consistently outperform the EKF in terms of correctness, robustness and ease of implementation (Kelly & Sukhatme, 2009; Van Der Merwe & Wan, 2004). Therefore, the use of a loosely coupled SPKS with a potentially dynamic sensor set such as that on-board the UAV provides an ideal filtering option.

To further improve the accuracy of the orientation estimates, the SPKS will be augmented with a novel algorithm that has been developed to include observations of orientation through the use of high definition video footage. The process used involves processing downward looking video footage using an algorithm that is similar to the Structure from Motion (SfM) technique often used in robotics or close range photogrammetry (Barazzetti et al. 2010). A post-processing based strategy allows for the optimal solution to be found through the use of a full bundle adjustment (Nagai et al., 2008). This inclusion of high definition video observation adds further redundancy and through direct observations of relative orientation provides greater accuracy in comparison to a traditional GPS/IMU positioning system.

The output of the GPS/IMU/Video SPKS is the position and orientation of the origin of the body frame within the ECEF Cartesian system. Considering this information, the next step within the LiDAR workflow requires the position and orientation of the laser system within the ECEF system to be known, which is reliant on the calibration parameters. Within a UAV LiDAR system the effect of errors within the boresight angles are minimised due to the low flying height. For instance, a boresight misalignment of 0.01^{o}, which results in an error of 1.31 m at a flying height of 700 m, will result in a horizontal error of only 0.005 m at typical UAV flying heights (30 - 120 m). The errors in the measurement of the lever arm offset, however, propagate directly into the accuracy of point position and need to be minimised by an appropriate calibration strategy. Conventional procedures for determining calibration parameters require a periodic survey of a well observed site (i.e. often an air field). However, the modularity of a UAV system suggests that the calibration parameters are likely to be significantly more dynamic and change between individual surveys. Therefore, a specific calibration procedure has been designed for this UAV. The procedure follows the three traditional stages of calibration for a LiDAR system outlined by Habib et al. (2010). For the purposes of this study the accuracy of the system calibration of the UAV will be considered to be equal to a full scale system based on simulation of the designed calibration strategy.

3. Results

The propagation of error into LiDAR point clouds is usually based on the flying conditions and error expected within a state-of-the-art LiDAR system at the time of publication. For example, Goulden & Hopkinson (2010) reports on the error within a LiDAR system based on the Optech 3100 scanner. The conditions of a UAV survey are, however, significantly different to full-scale surveys due to factors such as reduced flying heights and the greater inaccuracies of the miniaturised sensors. A comparison between the error contribution of each of the 17 components within a TerraLuma system and typical Optech 3100 setup (Table 2) highlights the inaccuracy associated with the measurement of angular quantities in low cost systems. Furthermore, table 3 outlines a comparison of other key variables often used as a measure for data quality in forest surveys, highlighting the exceptionally high point density (1000 pts/m2) of the system.

Table 2. A-priori standard deviation values of parameters within TerraLuma LiDAR System in comparison to a full scale system (adapted from Goulden & Hopkinson, 2010 and based on an Optech ALTM 3100 scanner)

Parameter	TerraLuma Value (1 σ)	Full Scale Value (1 σ)
σx, σy	0.03 m	0.03 m
σz	0.05 m	0.05 m
σω and σφ	0.2 - 0.5 °	0.005 °
σκ	0.2 - 0.5 °	0.010 °
$\sigma\omega_b$, $\sigma\varphi_b$ and $\sigma\kappa_b$	in σω , σφ & σκ	in σω , σφ & σκ
σx_L, σy_L and σz_L	0.01 m	0.01 m
σr	0.10 m	0.015 m
σβ	0.125 °	0.003 °
σB_h	0.020 °	0.014 °
σB_e	0.400 °	0.014 °

Table 3. A comparison of the key LiDAR variables between the TerraLuma UAV and an Optech ALTM 3100 scanner.

Variable	TerraLuma UAV	Full Scale System
Typical Flying height	50 m	1100 m
Scan Angle Range	-60 – 50	-25 – 25
Swath width at 25°	47 m	1300 m
Maximum Swath width	146 m	1300 m
Point Density	up to 1000 pt/m^2	3-15 pt/m^2
Laser footprint	0.07x1.40 m	0.27x0.27 m
Max. angle of incidence (flat terrain)	60	25

One of the key constraints within a low-cost system such as the TerraLuma UAV is the accuracy of the IMU. The IMU is essential to the system, providing the highest rate of measurement, tracking the position and orientation of the system in between the observations of accurate sensors. The IMU used within the TerraLuma system has been determined to have standalone short-term orientation accuracies in agreement to the manufacturer's specifications of 2 ^{o}. This accuracy is accompanied by significant bias instabilities and noise that are characteristic of a MEMs based IMU (which if uncorrected can result in a drift of up to 0.2 ^{o} per second). The result of considering observations of orientation made by a drift-free IMU ($\sigma\omega$, $\sigma\varphi$ and $\sigma\kappa$ = 2 ^{o}) on the accuracy of the LiDAR measurements can be seen in Figure 2. This figure demonstrates that the error due to poor estimates of orientation contributes up to 98% of the total error budget.

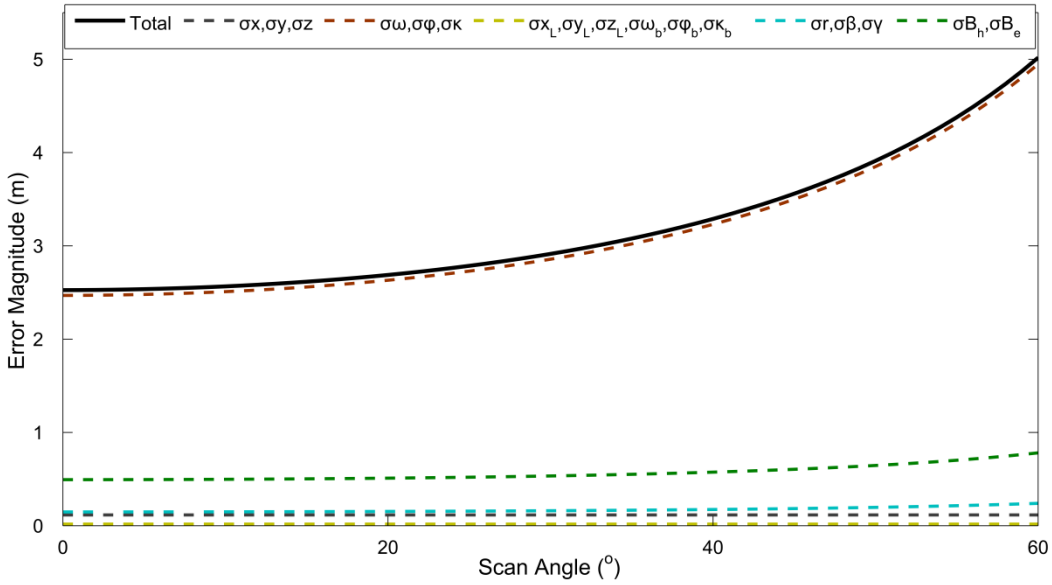

Figure 2. The effect of all error sources within the TerraLuma UAV LiDAR system on the point positioning accuracy of the LiDAR measurements, considering the worst case system errors and a flying height of 50 m.

The conventional method for constraining the error within the observations of orientation is to make use of additional observations from a GPS receiver. The GPS receiver on board the UAV makes high accuracy observation of position at a lower rate (20 Hz) than the IMU. Therefore, the use of a well designed integration strategy that constrains the IMU errors at each GPS observation can provide improved orientation estimates at the higher rate of the IMU observations. Under such a strategy, it has been shown that the errors in the observations of pitch and roll ($\sigma\omega$ and $\sigma\varphi$) can be reduced to 0.5 ^{o} and to 1.5 ^{o} in the yaw observation ($\sigma\kappa$) (Du, 2010). Although this resulting in a significant reduction in error, orientation is still the primary source of error (as shown in Figure 3).

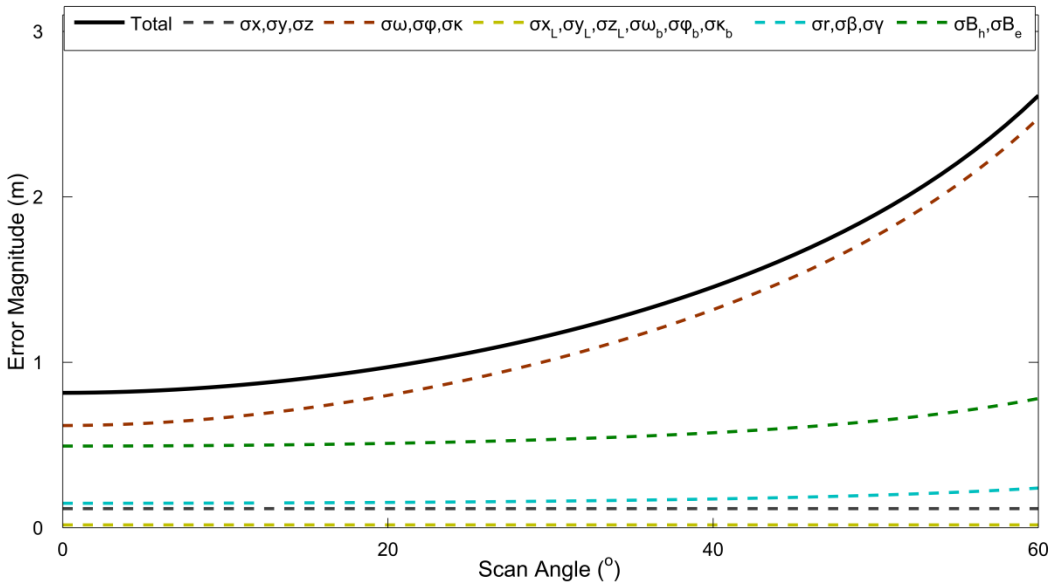

Figure 3. The result of a GPS/IMU filtering strategy constraining orientation error, to 0.5° in pitch and roll and 1.5° in Yaw, at a flying height of 40 m resulting in a higher overall LiDAR point positioning accuracy.

Orientation estimates from the outlined SfM routine can be used to further constrain orientation errors. Initial experiments of the novel algorithm developed for this research has shown significant improvements in the estimates of yaw and smaller improvements in the estimate of pitch and roll. Based on these initial tests, orientation estimates are expected to be reduced to within a range of 0.2 to 0.5 °. Figure 4 shows that the contribution of error from orientation is now within a similar range to the contributions of other system components. The primary error contributions can now be attributed to both the vertical beam divergence of the Ibeo LUX system and the orientation errors. It is noted that the Ibeo LUX has a high vertical beam divergence to ensure full coverage of the scanned area for its intended short range application in automation and this error component is fixed.

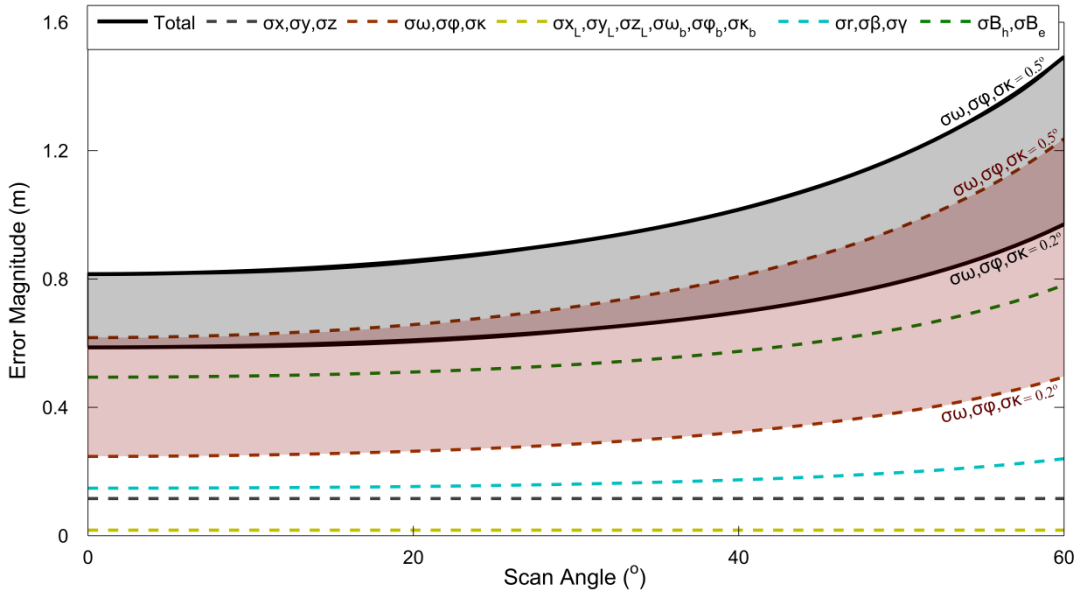

Figure 4. The expected result of improved orientation measurements due to the inclusion of HD video and Kalman filtering within the on-the-point positioning accuracy of the TerraLuma LiDAR system.

The point positioning error present within the observations made by the TerraLuma platform has been shown to increase with scan angle (Figures 2-4). Considering the high beam divergence of the Ibeo LUX scanner, the other dominant variable affecting the accuracy of the LiDAR observations is flying height (demonstrated in Figure 5). The magnitude of horizontal error towards the edges of the scan angle range increases by an order of magnitude between flying heights of 30 and 120 m. This effect is least pronounced at the centre of the scan suggesting that if increased flying heights are to be used the scan angle of the LiDAR system should be constrained. Furthermore, increased flying heights also result in significant decreases in the density of the measured point cloud.

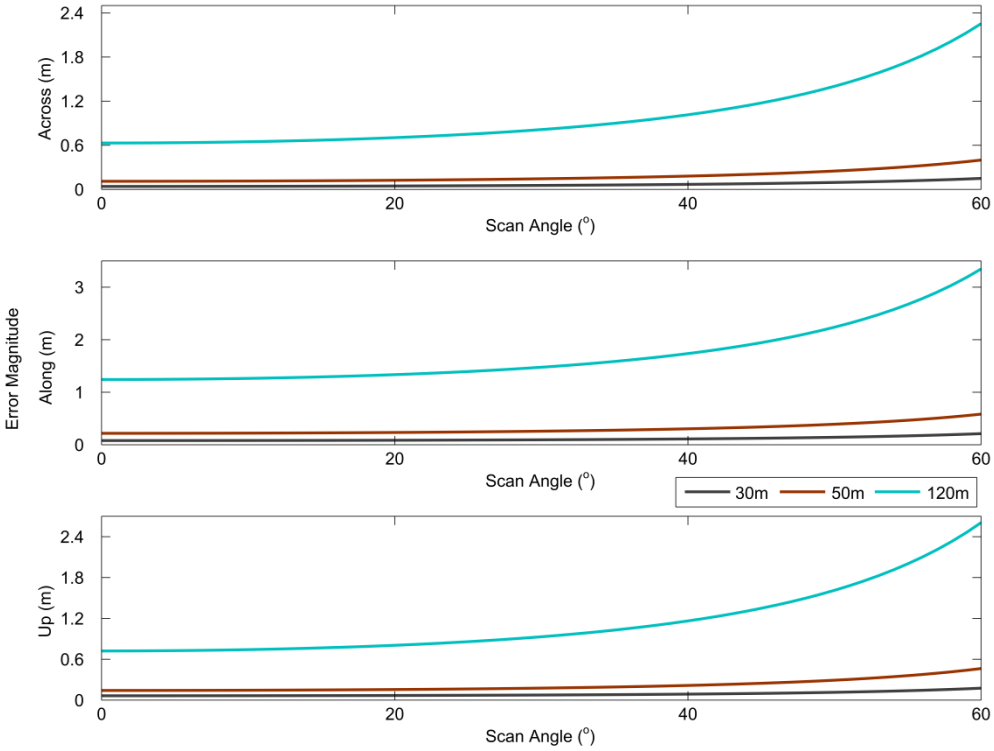

Figure 5. The accuracy of the TerraLuma LiDAR system based on the error statistic presented in Table 1 (σω, σφ and σκ = 0.35 °) and at flying heights of 30 m, 50 m and 120 m.

The cumulative effect of the errors, as a function of scan angle, within the TerraLuma system (flying at 50 m) in comparison to a typical full scale system flying at 1100 m is illustrated in Figure 6. The full scale system modelled is the Optech ALTM 3100 scanner (properties given in Table 2 and 3) which has a scan angle range of +/-25 °, within which the accuracy of the UAV system is within an acceptable range of the full scale system.

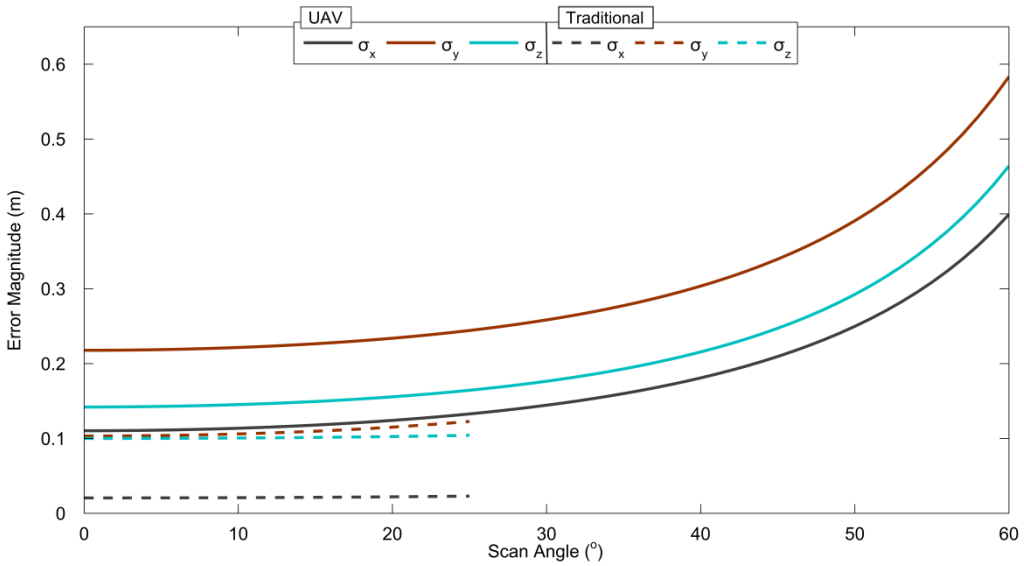

Figure 6. Accuracy of the TerraLuma LiDAR system (σω, σφ and σκ = 0.35 °) flying at 50 m in comparison to the accuracy of a traditional full scale system flying at 1100m (full scale system properties adapted from Goulden and Hopkinson, 2010).

4. Discussion

The use of a GPS/IMU/Video SPKS has allowed for a significant reduction in the error budget of the TerraLuma UAV LiDAR system. At a typical flying height of 50 m UAV-borne LiDAR can be expected to produce point clouds with sufficient accuracy for forest mapping. This accuracy, coupled with the increased point density achieved by the TerraLuma LiDAR system, presents a significant advantage for the fine-scale mapping of forests. The use of such a system will most likely result in a reduction in the underestimation of tree height measurements due to the highly dense point cloud being produced. Moreover, the modularity and low cost of the a TerraLuma LiDAR system will allow surveys to be conducted at a higher temporal frequency, allowing canopy closure rates and forest health to be monitored closely.

Several limitations of the use of a UAV-borne LiDAR system for forest measurement can also be determined from the results. The restricted flying height means that ground coverage is going to be significantly reduced and that the angle of incidence of a measurement towards the edge of the scan on the canopy will be increased. Although limited ground coverage is not necessarily a large restriction in the type of survey that would be designed for UAV platforms, increases in the angle of incidence would result in poor estimates of forest health indicators such as canopy closure and fraction cover. In order for UAVs to be used for this measuring this metric empirical correction based on other field measurements would be required.

The next stage in the development of the TerraLuma UAV is the collection and analysis of data over a forested test area. This will allow the capabilities of the system for forest mapping to be fully assessed and a set of survey designs to be developed with the aim of determining key forest indicators with potentially high temporal change such as forest health, bio-mass and canopy closure rates. Other future improvements to the system are reliant on advances in LiDAR technology, however, increased uptake of current technology could result in demand for an adaption of automotive laser scanners into lightweight scanners with smaller beam divergence for specific mapping purposes.

5. Conclusion

This study has demonstrated that a UAV-borne LiDAR using low-cost, lightweight sensors can produce point clouds with only slightly worse accuracies than full-scale traditional systems but with much higher point densities. It has been shown that improvements in the estimates of system orientation, produced through the use of a novel video augmented SPKS, has allowed for a low cost, light weight sensor suite to produce a point cloud of adequate accuracy for forestry mapping. Furthermore, by showing the achievable accuracy of a UAV derived point cloud, the implications and potential of such a platform for hyper-temporal resolution forest surveys, especially in the areas of change detection have been highlighted in this study.

References

Akay, A.E., Oğuz, H., Karas, I.R., & Aruga, K., 2009. Using LiDAR technology in forestry activities. *Environmental monitoring and assessment*, 151, 1, 117-25.

Baltsavias, E.P., 1999. Airborne laser scanning: basic relations and formulas. *ISPRS Journal of Photogrammetry and Remote Sensing*, 54, 2, 199 - 214.

Barazzetti, L., Remondino, F., Scaioni, M., & Brumana, R., 2010. Fully automatic UAV image-based sensor orientation. *International Archives of Photogrammetry, Remote Sensing and Spatial Information Sciences XXXVIII, Part 5 Commission V Symposium*. Newcastle upon Tyne, UK.

Berni, J. A. J., Zarco-tejada, P. J., Suárez, L., & Fereres, E., 2009. Thermal and Narrowband Multispectral Remote Sensing for Vegetation Monitoring From an Unmanned Aerial Vehicle. *IEEE Transactions on Geoscience and Remote Sensing*, 47, 3, 722-738.

Bouget, J., 2010. Camera Calibration Toolbox for Matlab®. Retrieved from http://www.vision.caltech.edu/bouguetj/calib_doc/.

Du, S., 2010. Integration of Precise Point Positioning and Low Cost MEMS IMU. Unpublished masters dissertation, *University of Calgary, Calgary*, Canada.

Eisenbeiss, H., & Zhang, L., 2006. Comparison of DSMs generated from mini UAV imagery and terrestrial laser scanner in a cultural heritage application, *International Archives of Photogrammetry, Remote Sensing and Spatial Information Sciences*, XXXVI-Part5, 90-96.

Glennie, C., 2007. Rigorous 3D error analysis of kinematic scanning LIDAR systems, *Journal of Applied Geodesy*, 1, 147-157.

Goulden & Hopkinson, 2010. The forward propagation of integrated system component errors within airborne LiDAR data, *Photogrammetric Engineering and Remote Sensing*, 76, 5, 589 – 601.

Habib, A., Bang, K.I., Kersting, A.P., & Chow, J., 2010. Alternative Methodologies for LiDAR System Calibration. *Remote Sensing*, vol. 2, No. 3, pp. 874-907.

Hunt Jr, E.R., Hively, W.D., Fujikawa, S.J., Linden, D.S., Daughtry, C.S.T., & McCarty, G.W., 2010. Acquisition of NIR-Green-Blue Digital Photographs from Unmanned Aircraft for Crop Monitoring. *Remote Sensing*, vol. 2, No. 1, pp. 290–305.

Hyyppä, J., Hyyppä, H., Leckie, D., Gougeon, F., Yu, X., & Maltamo, M. 2008. Review of methods of small-footprint airborne laser scanning for extracting forest inventory data in boreal forests. *International Journal of Remote Sensing*, vol. 29, No. 5, pp. 1339-1366.

Jaakkola, A., Hyyppä, Juha, Kukko, A., Yu, Xiaowei, Kaartinen, H., Lehtomäki, M. & Lin, Y., 2010. A low-cost multi-sensoral mobile mapping system and its feasibility for tree measurements. *ISPRS Journal of Photogrammetry and Remote Sensing*, vol. 65, No. 6, pp. 514-522.

Kelly, J., & Sukhatme, G. S., 2009. Visual-inertial simultaneous localization, mapping and sensor-to-sensor self-calibration. *2009 IEEE International Symposium on Computational Intelligence in Robotics and Automation*, Daejeon,Korea: 360-368.

Lichti, D.D., and Gordon, S. J., 2004. Error Propagation in Directly Georeferenced Terrestrial Laser Scanner Point Clouds for Cultural Heritage Recording, *Proceedings of FIG Working Week 2004*, Athens, Greece.

Lim, K., Treitz, P., Wulder, M., St-Onge, B., & Flood, M., 2003. LiDAR remote sensing of forest structure. *Progress in Physical Geography*, 27, 1, 88-106.

Lin, Y., Hyyppä, J., & Jaakkola, A., 2011, Mini-UAV-Borne LIDAR for Fine-Scale Mapping. *Geoscience and Remote Sensing Letters, IEEE*, 8, 99, 426–430.

May, N., & Toth, C., 2007, Point positioning accuracy of airborne LiDAR systems: A rigorous analysis. *International Archives of Photogrammetry, Remote Sensing and Spatial Information Science*, 36, 107–111.

Morin, K. W., 2002, Calibration of airborne laser scanners, Unpublished Masters dissertation, *University of Calgary, Calgary, Canada*.

Morsdorf, F., Nichol, C., Malthus, T., & Woodhouse, I.H., 2009. Assessing forest structural and physiological information content of multi-spectral LiDAR waveforms by radiative transfer modelling. *Remote Sensing of Environment*, 113, 10, 2152-2163.

Nagai, M., Chen, T., Ahmed, A., & Shibasaki, R., 2008. UAV Borne Mapping by Multi Sensor Intergration. *The International Archives of the Photogrammetry, Remote Sensing and Spatial Information Sciences, Part b1 XXXVII*, Beijing, China: 1215-1222.

Schaer, P., Skaloud, J., Landtwing, S., & Legat, K., 2007. Accuracy estimation for laser point cloud including scanning geometry. *5th International Symposium on Mobile Mapping Technology (MMT2007), Padua, Italy*.

Van Der Merwe, R., & Wan, E. A., 2004. Sigma-point Kalman filters for integrated navigation. *Proceedings of the 60th Annual Meeting of the Institute of Navigation (ION)*, Ohio, USA: 641–654.

Zhang, H., Wu, Y., Wu, M., & Hu, X., 2010, Improved multi-position calibration for inertial measurement units, Measurement Science and Technology, 21.